Enhanced on-chip SERS based biomolecular detection using electrokinetically active microwells†

Yun Suk Huh, Aram J. Chung, Bernardo Cordovez and David Erickson*

Received 9th June 2008, Accepted 13th October 2008
First published as an Advance Article on the web 12th November 2008
DOI: 10.1039/b809702j

Here we present a novel microfluidic technique for on-chip surface enhanced Raman spectroscopy (SERS) based biomolecular detection, exploiting the use of electrokinetically active microwells. Briefly, the chip comprises of a series of microfluidic channels containing embedded microwells that, when electrically actuated, either locally attract or repulse species from solution through a combination of electrokinetic effects. We demonstrate that the approach combines the advantages of existing homogeneous (solution phase) and heterogeneous (surface phase) on-chip techniques by enabling active mixing to enhance the rate of binding between the SERS enhancers and the biomolecular targets as well as rapid concentration of the product for surface phase optical interrogation. This paper describes the chip design and fabrication procedure, experimental results illustrating the optimal conditions for our concentration and mixing processes, and a numerical analysis of the flow pattern. To demonstrate the usefulness of the device we apply it to the quantitative detection of nucleic acid sequences associated with Dengue virus serotype 2. We report a limit of detection for Dengue sequences of 30 pM and show excellent specificity against other serotypes.

1. Introduction

Surface-enhanced Raman spectroscopy (SERS) is a powerful vibrational spectroscopy technique. The phenomenon occurs when a target molecule is brought into close proximity with a metallic surface containing nanoscopically defined features or in solution next to a metallic nanoparticle with a diameter much smaller than the wavelength of the excitation light.[1] When light at the resonant wavelength is incident on the surface or particle, a plasmon mode is excited which locally enhances the electromagnetic energy in the vicinity of the target molecule, significantly enhancing the strength of the Raman scattered light. This output is molecularly specific[2] and as such the spectrum obtained from SERS analysis provides much more detailed information about the molecular structure of the target molecule than those obtained using other spectroscopic techniques (such as fluorescence[3–5]). Though Raman scattering is traditionally used for chemical detection and analysis,[6,7] it has recently become popular for biological and biomolecular applications[3,8–10] including single molecule analysis.[11,12] To exploit these advantages, a number of research groups have recently developed microfluidics based SERS chips.[9,10,13–16] In general, the advantages of microfluidic SERS analysis are reduced sample size, shorter reaction times and improved yield when compared to conventional techniques.[1–8]

Sibley School of Mechanical and Aerospace Engineering, Cornell University, Ithaca, NY, 14853, USA. E-mail: de54@cornell.edu; Fax: +1 607-255-1222; Tel: +1 607-255-4861

† Electronic supplementary information (ESI) available: Illustration of electroactive microwell device for SERS based nucleic acid detection (Fig. S1), finite element simulations of the transport process of mixing (Fig. S2), and plot of normalized peak intensity as a function of concentration (Fig. S3). See DOI: 10.1039/b809702j

Broadly speaking there are two ways in which a SERS detection reaction can be carried out on chips: homogeneously, where the target becomes bound or absorbs onto the solution phase metallic nanoparticles which act as Raman enhancers,[9,16] or heterogeneously, where the solution phase targets interact with the surface phase SERS active clusters such as roughened electrodes,[17] or precipitated silver and gold nanoparticles (NPs).[18,19] The former of these has the same advantages as all homogeneous reactions (*i.e.* faster reaction rate and relative ease of implementation) as well as enhanced uniformity and repeatability of the SERS enhancement since the nanoparticles can be synthesized with high uniformity. As an example of such an implementation, Park *et al.*[9] described the use of an alligator-teeth-shaped PDMS microchannel to promote mixing between the target analyte and the metallic colloids used as SERS enhancers. One disadvantage of the homogeneous approach however is that because the Raman enhancers are dispersed in solution, detection sensitivity are relatively low (unless enhanced microscopy techniques like confocal are used). Heterogeneous reactions using SERS active substrates such as metal-film-over-nanospheres[20] and nanowells,[21] have also been recently reported. While these systems can have fundamentally greater sensitivity (essentially concentrating the detection zone from 3D to 2D), the analysis time is typically longer (since the molecules must diffuse to the analysis site), the chip fabrication is more complicated (since nanoscopic features must be patterned) and in some cases it is difficult to obtain regular and repeatable SERS enhancement.

To address this, a number of authors have recently developed unique "optofluidic" based on chip SERS devices.[22,23] For example techniques, Measor *et al.*[24] used liquid core optical waveguides to confine the electromagnetic energy lengthwise though a hollow microchannel, allowing it to interact with

a greater number of particles. Analogously, Wang *et al.*[10] used a nanochannel trap to collect solution phase Raman particles at a junction between a micro- and nanochannel. In the first of these approaches, the light/particle interaction is increased but the scattered light is still dispersed and thus the signal capture efficiency may be low. The second case allows for physical concentration of the Raman enhancers but requires transport through a nanochannel, potentially limiting throughput.

In this paper we present a novel microfluidic SERS detection chip that combines the advantages of homogeneous and heterogeneous based detection systems without the limitations of existing devices as outlined above. Briefly, our approach is based on the use of electrokinetically active microwells[25] which serve to both enhance mixing between the target and solution phase Raman enhancers[26–28] and then physically concentrate the product for more sensitive and rapid optical interrogation.

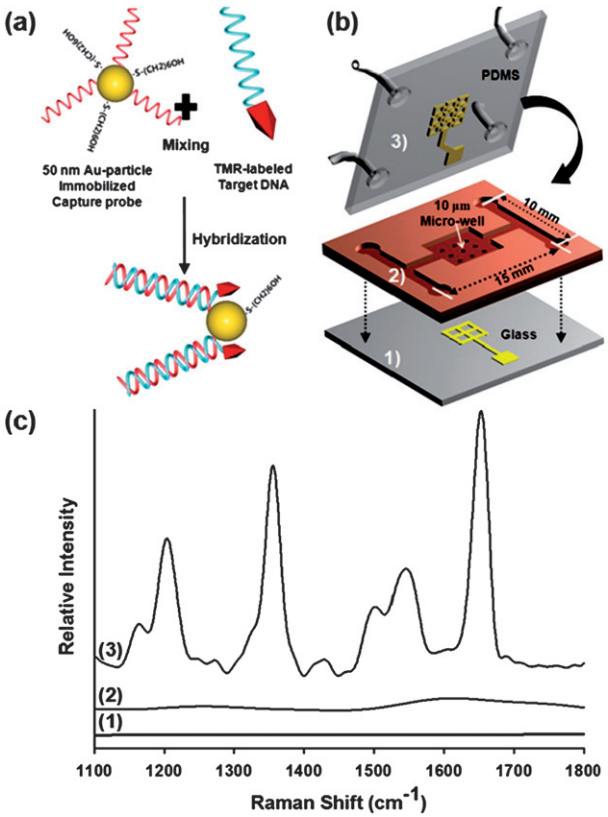

Fig. 1 (a) Schematic illustration of the DENV-2a hybridization reaction, 50 nm gold NPs used as SERS enhancers, and technique for limiting non-specific adsorption. (b) Overview of chip fabrication process: 1) Ti/Au was deposited onto Pyrex glass substrate as a lower electrode. 2) Microwells with 10 μm size were fabricated with 8 μm thickness of polyimide dielectric layer and an additional polyimide layer was inserted to form microfluidic channel. 3) Au was transferred onto the PDMS layer as a upper electrode. Final device dimensions are 10.0 (width) × 15.0 (length) × 0.16 (height) mm. (c) SERS spectra of the DENV-2a hybridization reaction procedures. (1) SERS spectra of gold NPs after immobilization of capture probes and application of MCH to protect against non-specific absorption. (2) SERS spectra after hybridization with DENV-4a (negative control) and (3) with DENV-2a (target DNA) using the functionalized gold NPs. The concentration of each target DNA in hybridization reaction is 3 nM.

A schematic of the chip is shown in Fig. 1b and Fig. S1.† In this paper we detail the chip design and demonstrate its usefulness by applying it to the sensitive and specific detection of nucleic acid sequences associated with Dengue virus.[29,30] In addition we have experimentally quantified both the rate and degree of physical concentration in the wells as a function of the applied potential. A numerical analysis of the flow/transport patterns during the mixing stage is also presented. Using the Dengue probes we demonstrate the quantitative nature of the detection method and characterize the limit of detection of the device.

2. Materials and methods

2.1 Chemicals

All chemicals and solvents were purchased at the highest purity grade available. For the SERS enhancers, 50 nm diameter gold colloid solutions were purchased from Nanocs (New York, NY) and were diluted to a final concentration of 0.3 nM in 10 mM phosphate-buffered saline (PBS) buffer solution (0.6 M NaCl, pH 7.4). In this study, Dengue virus serotype 2 (DENV-2) has been chosen as the target analyte. There are four closely related but antigenically distinct serotypes (DENV-1–4) which threaten a major public health in >100 countries and infect an estimated 50 million people annually.[30] Two oligonucleotides (denoted as DENV-2a and DENV-4a, respectively), which contain sequences from DENV-2 and DENV-4 were purchased from Operon Biotechnologies (Huntsville, AL). The capture probe for DENV-2a was 3′ modified with a thiol-modifier containing C3 S-S functionality and had the following sequence: 5′-ATG AAG CTG TAG TCT CAC TGG AAG G C3 S-S-3′. We confirmed the specificity of the SERS detection technique by conducting hybridization reaction using the target DNA, DENV-2a for positive control and DENV-4a for negative control. The target probe was modified with TAMRA dye at the 5′ end. The sequences of DENV-2a (positive control) and DENV-4a (negative control) oligonucleotides are (TAMRA) 5′- TCT AGT *CCT TCC AGT GAG ACT ACA GCT TCA T*CT CAC CTT G-3′, (Cy3) 5′- CTA GTC *CTT CCA CCA GGA GTA CAG CTT CCT C*CT GGC TTC G-3′, respectively. The italicized portions of the target sequence are the complementary nucleotides to each capture probe. Stock DNA solution at a base concentration of 300 μM were prepared using 10 mM PBS buffer and stored in a freezer until use. Poly(dimethylsiloxane) (PDMS) microfluidics were made using a Sylgard® 184 silicon elastomer kit (Dow Corning, Midland, MI).

2.2 Preparation of DNA functionalized gold nanoparticles and hybridization reaction

Fig. 1(a) shows a schematic of a functionalized gold NP and hybridization reaction along with an exploded view of the Raman enhancement chip used here. In this experiment 50 nm diameter gold NPs were functionalized with the capture DNA.[3,31] To immobilize the probe, 300 nM of the thiolated capture DNA was added to 0.3 nM Au colloid solution in PBS buffer solution. The reaction was allowed to proceed for 4 h at room temperature, followed by a 1 h exposure to 300 μM 6-mercapto-1-hexanol (MCH). Because MCH forms well-organized self-assembled monolayers (SAMs) on the surface, non-specifically adsorbed

ssDNA is displaced, and chemically attached the thiol modified ssDNA reorients itself, making the majority of surface-bound probes accessible for hybidization.[32] A centrifugation/resuspension cycle was then repeated twice for through removal of excess reagents. The centrifugation was carried out at 10 000 rpm for 30 min. The gold NPs immobilized capture probe were resuspended to the final concentration of 3 nM capture probe in hybridization buffer and then introduced into the sample inlet port of SERS device (see ESI†) at the flow rate of 5 μL s^{-1}. Simultaneously, the TAMRA labeled target DNA in PBS buffer solution flown in through another port also at a speed of 5 μL s^{-1}. The two microfluidic channels merged, mixing the two streams as they were flown towards the microwell site with the attraction voltage applied (see Fig. S1d and e†). After a fixed collection period, additional mixing was initiated by applying an alternating current condition of 1.0 V. In all cases a Hewlett–Packard 6234A dual output power supply and a Keithley 236 were used to apply and measure these potentials. PBS buffer solution was then flown over the well at the flow rate of 5 μL s^{-1} to remove non-specifically bound target. Subsequently, the electroactive microwells were probed with a 785 nm laser excitation source using a commercial Raman microscope and spectrometer (see Section 2.4 for details). For the florescent microsphere experiments, transport was recorded using Unibrain Fire-i™ software and a Sony XCD-X710 camera.

2.3 Microfabrication procedure

Fig. 1b shows the chip assembly procedure. The device consisted of three functional layers namely a lower electrode, a polyimide (PI) dielectric, and an upper electrode. In this device, Pyrex glass was used as a bottom electrode substrate. First, the Pyrex glass was coated with positive photoresist S1813 (Shipley, Marlborough, MA) at 4000 rpm for 30 s. The coated glass was soft baked for 1 min at 90 °C and exposed to 75 mJ/cm^2 of 300 to 500 nm ultraviolet light through a mask of the desired pattern. The exposed glass was soaked in Toluene for 60 s, and post baked for 15 s at 90 °C. It was then dipped in developing solution (1 part Shipley Microposit 351 concentrate to 5 parts DI water) for 28 s, rinsed in a DI water overflow chamber for 1 min, and dried with N_2 gas. Following this, 5 nm Ti/50 nm gold was evaporated and a lift off process carried out with 1165 photoresist stripper (Shipley Microposit) overnight, forming the lower electrode on the glass surface. As shown in Fig. 1b, the HD-8820 PI (DuPont) middle layer has a step structure which consisted of a lower passivation layer and an upper microfluidic channel. The PI passivation layer was deposited on the topside of the glass substrate patterned with the lower electrode, which served to electrically isolate the electrode from the electrolyte solution when the electric field was applied. The photosensitive PI was spun on at 1400 rpm for 60 s and soft baked for 3 min at 120 °C. It was patterned with 450 mJ/cm^2 exposure and developed using 2.38% TMAH solution (AZ 300 MIF) for 3 min. Curing was done by temperature step gradient of 130 °C, 170 °C, 250 °C, and 320 °C for 4 h in a programmable oven. When complete the lower PI layer has an 8 μm depth which represented a ~25% thickness loss in the unexposed areas due partial etching by the developer. When solutions were introduced into the chip then, the only electrode locations that were exposed to it were the bottom of the microwell and the upper electrode surfaces. The microfluidic channel in the upper PI layer was fabricated using the same procedure.

To fabricate the upper gold electrode patterned PDMS layer we used a similar technique to that described by Lee *et al.*[33] 50 nm thick gold features were first patterned on a silicon substrate. After the gold features were created, an MPTMS (3-mercaptopropyl-trimethoxysilane) film was deposited onto the top surface of the wafer using molecular vapour deposition (MVD). The MPTMS layer served as an organic adhesion layer aiding with the transfer of the gold features from the silicon wafer to the PDMS. For the bonding of the gold patterned PDMS and the glass substrate patterned by PI, the surfaces of both layers were activated in oxygen plasma. The two halves were aligned using our home-made aligner.

2.4 Raman spectroscopic measurements

Raman measurements were made using a Renishaw inVia Raman microscope spectrometer coupled to a Leica microscope. The experiments were conducted by focusing the excitation laser on the electro-active microwell. The diode laser used here had an excitation wavelength of 785 nm and operated at approximately 10 mW of power. Wave-number ranges from 1100 cm^{-1} to 1800 cm^{-1} were examined here. A 50× long working distance objective lens was used with a spot size of 2 μm.

3. Results and discussion

The ability to handle and concentrate nanoparticles on-chip is important for a number of biomolecular detection applications. As mentioned above, the electrokinetic SERS device developed here allows for both efficient mixing to enhance the reaction rate and concentration to enhance detection sensitivity through the use of electroactive microwells.

To quantify the concentration capability of this device, 44 nm carboxylate functionalized fluorescent polystyrene (PS) beads in 10 mM PBS buffer were introduced into the chip through the inlet port (Fig. S1†). The PS beads had a negative ζ potential of −41 mV as reported by Nemmar *et al.*[34] After introduction of the nanoparticles into the chamber, the electric field was applied between the upper and lower gold electrodes attracting the nanoparticles into the 10 μm diameter well. The local nanoparticle concentration in the well was estimated using the gray scale intensities from the experimental images which were analyzed for 10 s using image-analysis software (Scion Image, Scion Corp., Frederick, MD). The efficiency of concentration was analyzed through the results obtained by using three different devices. Fig. 2 shows the average florescent intensity in the well as a function of time for applied attraction voltages ranging from 0.5 V to 2.0 V. The lines shown in the image represent the average of three separate measurements. As shown in Fig. 2, the rate of concentration increases with higher applied potentials. Note that for all the higher applied potentials the well reached a saturated concentration condition within 3 s. At the lower potentials (0.5 V and 0.75 V) however a steady state was reached within the same amount of time but at a lower steady state concentration. Our previous results[25] on trapping stability in a quiescent medium showed that the trap stability can be

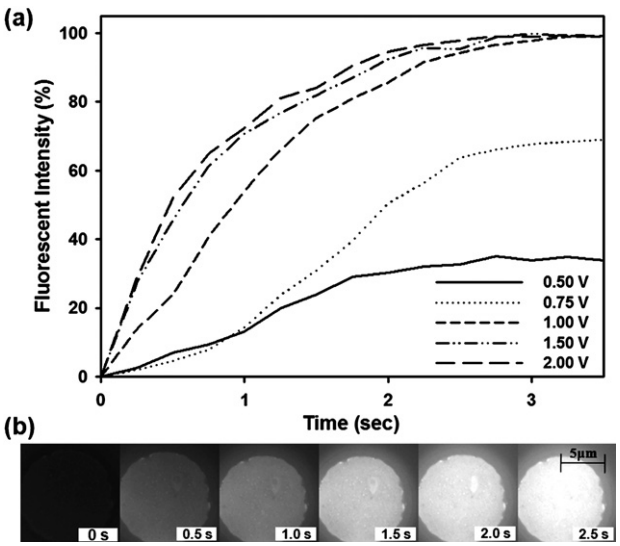

Fig. 2 (a) Efficiency of concentration for 44 nm PS particles into a 10 μm diameter with different applied potentials. (b) Time-lapse captured concentration images of 44 nm fluorescent PS particles from the bulk solution into the well for 2.5 s under a 1 V applied potential.

estimated by comparing the work required to dislodge a particle from the well with the random thermal energy in the system, represented by k_bT, *via* $S = qEh/k_bT$ (where S is a non-dimensional stability parameter, q is the charge on the particle, E is the local potential field strength in the well, and h is the height of the well). Specific well occupancy was observed to be much higher under the same experimental conditions. Smaller wells get filled more since field concentration increases with decreasing well diameter, thus generating a stronger trapping force (see Cordovez *et al.*[25]).

In addition, the electrokinetic movement of PS particles by electrophoresis depends on differences in the migration velocity of the PS particles through the given medium under applied potential conditions. The drift velocity of a charged PS particle is expressed as the following equation: ($\boldsymbol{V}_{d,i} = \boldsymbol{\nu}_i \times F_{E,i}$, where $\boldsymbol{\nu}_i$ and $F_{E,i}$ indicate the electrophoretic mobility of PS particles and force per PS particles by the electric field, respectively). Thus, as expected, the higher the potential that was applied between the upper PDMS electrode and the lower microwell electrode, the larger drift velocity of PS the particles had. This means that the PS particles of the highest potential are concentrated to the microwell, along with faster velocity (Fig. 2a). Based on these measurements a potential strength of 1.0 V was chosen as a suitable condition for the Raman measurements, and thus will be applied for the rest of the study. To assess this device, the mixing process for hybridization reaction and the washing step was estimated using 44 nm PS particles in 10 mM PBS buffer solution. Fig. 3 shows the time-dependent images of trapping and rejection in a 10 μm well by applying the potential condition of 1V. Similar to the results described above, 44 nm PS particles were drawn from the bulk solution into the microwell when applied using a positive voltage on the bottom electrode (Fig. 3a–3c). Immediately following the concentration of PS particles, the applied potential field is switched to be ejected by reversing the polarity (Fig. 3d and 3e). The switching speed was approximately 2 s consistent with the time required to obtain >66% concentration of the particles in the wells. As can be seen, the microwells allow for active repulsion of the trapped target particles by reversing the polarity of the applied potential.

To examine the electrokinetic transport processes involved in the mixing stage for washing and hybridization, a three-dimensional finite element model (FEM) of the system was constructed using the COMSOL finite element package. The computational domain used here matched exactly that shown in Fig. 1b, which contains the microwell and a chamber domain. Details of the modelling procedures and general assumptions are available in earlier works.[35] Briefly however, we model the system with incompressible Stokes flow equations ($\eta\nabla^2\boldsymbol{v} - \nabla p = 0$, where $\boldsymbol{v}$ is the flow field, η is the viscosity and p is the pressure), continuity equations ($\nabla\cdot\boldsymbol{v} = 0$), and use a simple Laplacian to model the applied electric field ($\nabla^2\phi = 0$, ϕ is the applied potential). The Stokes flow and continuity equations were subject to electroosmotic slip, v_{eo}, conditions at the wall of microwell and the two side walls of the chamber. The slip velocity was calculated using the Helmholtz–Smoluchowski equation $\boldsymbol{v}_{eo} = -\varepsilon\zeta\boldsymbol{E}/\eta$, where ε is the permittivity of the medium, ζ is the surface zeta potential set here as −40 mV,[36] and $\boldsymbol{E}$ is the field strength ($\boldsymbol{E} = -\nabla\phi$). The normal flow condition ($\boldsymbol{v}\cdot\boldsymbol{n} = 0$) was given for the remaining two side walls of the chamber since no pressure was applied during the mixing processes. For the polystyrene fluorescent microspheres used here the electrophoretic mobility was computed using $\boldsymbol{v}_{ep} = \varepsilon\zeta_p\boldsymbol{E}/\eta$ with $\zeta_p = -41$ mV.[34,37] The net electrokinetic transport streamlines were computed from the summation of the electroosmotic and electrophoretic velocity $\boldsymbol{v} = \boldsymbol{v}_{ep} + \boldsymbol{v}_{eo}$ and shown in the ESI Fig. S2.† From these results it can be clearly seen that the applied potential (top electrode: ground, bottom electrode: 1.0 V) induces a strong trapping potential, dragging the particles from the chamber into the microwell; however when reversing the potential polarity, the concentrated particles were ejected as illustrated in Fig. S2b.† These numerical trapping/

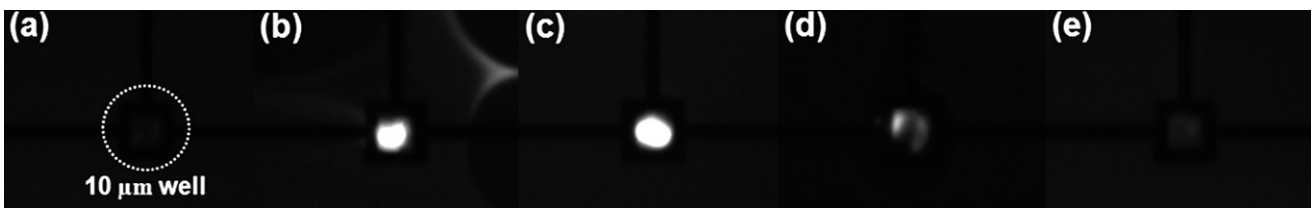

Fig. 3 Time-lapse images of concentration and ejection of 44 nm PS particles in a 10 μm well under 1.0 V potential. (a) Inactive microwell, (b) particle attraction begins and beads are drawn into well, (c) microwell after 5 s of attraction, (d) particles are ejected from the well by reversing the polarity, (e) microwell after 5 s rejection.

repulsion analysis results are consistent with the experimental observations represented in Fig. 3.

4. On-chip surface enhanced raman scattering based detection of Dengue virus sequences

Many SERS studies are aimed at understanding colloid aggregation/concentration during and prior to SERS measurement as it plays an important role in determining reproducibility.[38,39] Tantra *et al.*[40] have been recently reported that data reproducibility was improved by increasing vortexing time during the aggregation step. Such improvements were thought to be associated with the formation of reproducible metal clusters under conditions of forced convection, so as to reduce the effect of random collision governed by natural convection.

Using the working principle described above, we have developed a device for rapid, quantitative SERS based nucleic acid detection. The device exploits the mixing mechanism to increase the reaction rate (and thereby reduce the analysis time) and the electrokinetic concentration technique to decrease the limit of detection.

As detailed in the Methods and materials section, the target DNA and gold NPs immobilized with capture probes were introduced into the chip *via* their respective inlet ports into the chamber chamber, where mixing was performed as follows. The gold NPs were first attracted into the well for 5 s at an applied potential of 1 V and then the polarity reversed and the rejection potential applied for a further 5 s. The process was repeated a fixed number of cycles as will be described in detail later. After the mixing step, DNA hybridized gold NPs were washed to remove the excess nonspecific target probes by flowing PBS buffer solution at a flow rate of 5 μL s^{-1}. In the final step the reaction products were consistently concentrated in the microwell by applying the attraction potential. This final concentration step was found to increase the reproducibility and intensity of SERS signal by controlling the mixing and concentration of the SERS active clusters. To obtain the SERS signal, the excitation laser was focused at the microwell and the spectrum recorded integration time set to 15 s. Device to device reproducibility of the system was also verified by comparing the peak area of 3 nM positive sample (Fig. 1c(3)) at 1653 cm^{-1}, 1360 cm^{-1} and 1219 cm^{-1} of the ouput SERS spectra. In all cases good agreement was found.

To characterize the reaction/device specificity, SERS detection experiments were conducted using nanoparticles functionalized with probes specific to DENV-2 and introducing (in separate experiments) DENV-2a and DENV-4a targets. For the results presented here we obtained spectra from 3 different points in the well (using a 2 μm laser spot size) and did not find any significant difference in the output spectra. As shown in Fig. 2 and 3 for the 10 μm diameter-well the local nanoparticle concentration is relatively uniform and thus this level of consistency can be expected.

Fig. 1c shows the SERS spectra collected on-chip for (1) no target DNA, (2) DENV-4a (negative control) and (3) DENV-2a (positive control). In the latter two cases the concentration of targets in solution was 3 nM. As can be seen in Fig. 1c **(1)** and **(2)**, our results show that almost no detectable Raman signal was observed from the control gold NPs, nor the gold NPs hybridized with DENV-4a. As expected, Fig. 1c **(3)** shows the correct spectroscopic fingerprints corresponding to TAMRA-labeled DENV-2a.

As outlined above, each mixing cycle requires approximately 10 s to complete, thus determining the optimal number is important to minimizing the amount of time required to perform the detection. To find the optimum conditions here, the number of the mixing cycle was varied in the range of 10, 20, 40, 60 and 80 cycles. Fig. 4a shows the Raman spectra of TAMRA-labeled DENV-2a at each of these points. In order to quantify the mixing performance, the change in the area of the SERS peak from 1610 to 1700 cm^{-1} was monitored. As can be seen in Fig. 4b, as the number of mixing cycle increased, the SERS signal intensity increased suggesting more of the nucleic acid was captured by the nanoparticles. The calibration curve in Fig. 4c pertains to the area under the primary diagnostic peak at 1653 cm^{-1} of the ouput SERS spectra. We obtained this peak area using the WIRE™ 2 program. This is consistent with the techniques used by Lee *et al.*[41] for SERS detection. On the basis of the measured peak area the hybridization reaction was about 35% complete after 20 cycles. After 40 cycles, over 80% of reaction was completed. Above 60 mixing cycles only marginal increases in the SERS peak area were observed suggesting the reaction had gone to completion.

To characterize the limit of detection (LOD) of the system, a concentration study was carried out. Fig. 5 shows the SERS spectra of TAMRA-labeled DENV-2a onto gold NPs in a microwell with the different concentrations of target probe (3 pM, 30 pM, 300 pM and 3000 pM). As shown in Fig. 5a, characteristic Raman peaks for the TAMRA-labeled target DNA were observed as similar to previously reported results.[3,4,9] In this

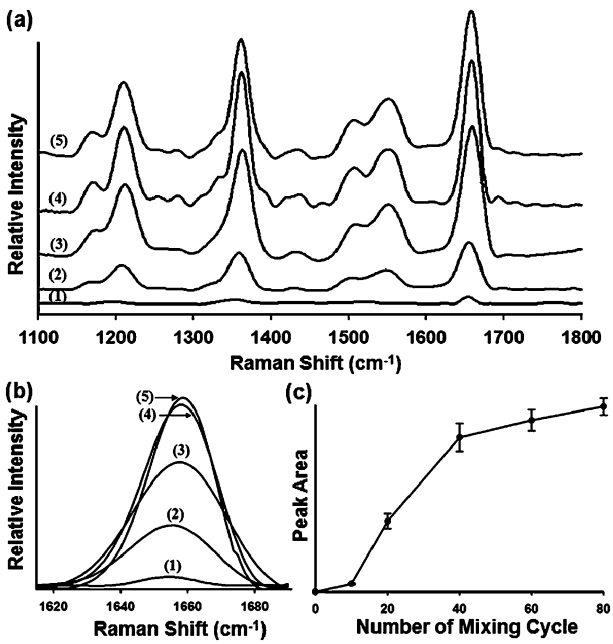

Fig. 4 (a) SERS spectra of TAMRA-labeled Dengue virus serotype 2 with increasing the number of mixing cycles. (1) 10 cycles, (2) 20 cycles, (3) 40 cycles, (4) 60 cycles, and (5) 80 cycles. (b) SERS spectra from 1610 to 1700 cm^{-1} corresponding to each case illustrated above. (c) The variation in Raman peak as a function of mixing cycle. The concentration of target DNA was 3 nM.

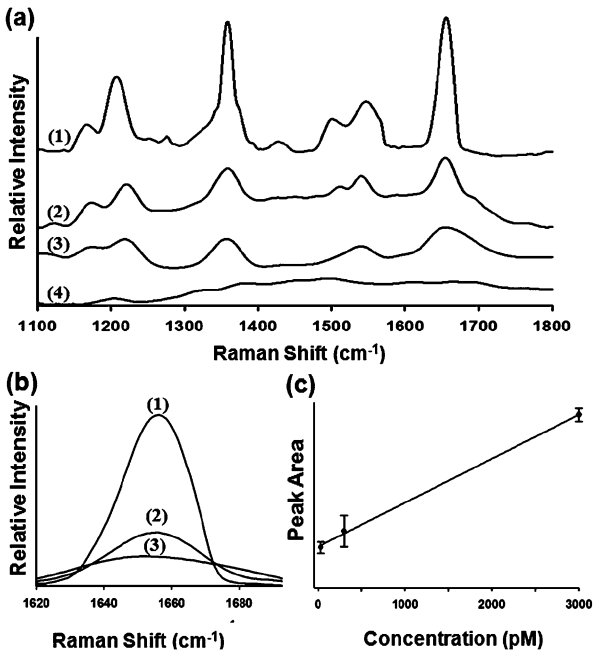

Fig. 5 (a) SERS spectra of TAMRA-labeled DENV-2a onto the gold NPs at different concentrations. Under applied potential, gold NPs was trapped to form SERS-active clusters with predictable position in 10 μm well. (1) 3000 pM, (2) 300 pM, (3) 30 pM, and (4) 3 pM. Raman peaks for the TAMRA-labeled DENV-2a were found at 1653, 1543, 1505, 1360, 1219, and 1170 cm^{-1}. (b) SERS spectra from 1610 to 1700 cm^{-1} corresponding to each case illustrated above. (c) Plot of normalized peak area as a function of concentration (correlation coefficient: $R = 0.994$). Note that the 3 pM result is omitted from (b) and (c) since the concentration was below the limit of detection.

experiment, the Raman signal was taken after a final 10 s trapping time. As observed in Fig. 2a, the efficiency of concentration at 1.0 V is increased over time and was saturated above 3 s. Similar to the results shown in Fig. 4, the Raman peak from 1610 to 1700 cm^{-1} was used for quantitative evaluation. The corresponding calibration curve, based on the variations in the peak area, is displayed in Fig. 5b and 5c. As expected the intensity of the Raman peak increases concomitantly with increasing the concentration of target DNA (Fig. 5b). Fig. 5c shows the linear response of peak area with the increase in DNA concentration. The peak intensity did also increase monotonically with concentration (correlation coefficient: 0.990), but the response was not as linear as what was observed using the peak area approach (see Fig. S3†). Based on these results the limit of detection for our device was determined to be 30 pM.

In most SERS detection system, silver NPs were used as a SERS enhancer because of the relatively high SERS enhancement factors, 10^{10} for silver NPs *vs.* 10^{8} for gold NPs.[42] In this study, gold colloidal particles was used as SERS enhancing agents because of their long-term stability, easily controllable size distribution, and high homogeneity.[16] Even though the SERS detection was carried out by using the gold NPs, we successfully achieved similar or greater sensitivity compared to similar microfluidic SERS devices using silver NPs.[9,16,43]

The first SERS application to microfluidics was carried out by Keir *et al.*[44] The SERS substrate, silver nanocolloid, was prepared by borohydride reduction of silver nitrate in the microfluidic channel. Using this on-chip SERRS technique, it was possible to detect 10 fM of an azo dye analyte, derived from trinitrotoluene (TNT). Since the introduction of chip based SERS detection, Docherty *et al.*[45] and Lee *et al.*[9] reported LOD of dye-labeled DNA oligonucleotides were 100 nM and 10 pM, respectively, using silver NPs in a microfluidic chip. Other systems have also reported LODs around the 1–2 nM level.[16,41,43] In this work, an LOD of 30 pM was obtained, which comparable with the previously reported results using silver NPs.

5. Summary and conclusions

In this paper we have reported the development of an "opto-fluidic" SERS chip for the detection nucleic acid sequences associated with Dengue virus serotype 2 (DENV-2). We have demonstrated how electrokinetically active microwells embedded within the device could be used to both enhance solution phase mixing of the target nucleic acids and the Raman enhancers and provide sample concentration for greater detection sensitivity through a combination of electroosmotic and electrophoretic effects. The concentration performance of the device was characterized using 44 nm polystyrene nanoparticles and it showed enhancement of more than 90% within 2.5 s when potentials between 1 and 2 V were applied between an upper electrode and the bottom of the well. Using DENV-2a sequences, we successfully detected SERS signals with a limit of detection on the order of 30 pM. This new approach could provide a significant contribution to the ongoing efforts to miniaturize biomolecular analysis systems for fields such as pharmaceuticals testing and the detection of biological warfare agents.

Acknowledgements

The authors of this article are thankful for the financial support of the National Institutes of Health—National Institute of Biomedical Imaging and Bioengineering through grant number R21EB007031 to DE and the Korea Research Foundation Grant funded by the Korean government (MOEHRD)″ (KRF-2007-216-D00059 for YSH).

References

1 D. Graham, B. J. Mallinder and W. E. Smith, *Angew. Chem.*, 2004, **76**, 412.
2 R. Brown, W. E. Smith and D. Graham, *Terahedron Lett.*, 2001, **42**, 2197.
3 Y. C. Cao, R. Jin and C. A. Mirkin, *Science*, 2002, **297**, 1536.
4 R. Jin, Y. C. Cao, C. S. Thaxton and C. A. Mirkin, *Small*, 2006, **2**, 375.
5 N. A. Abu-Hatab, J. F. John, J. M. Oran and M. J. Sepaniak, *Appl. Spectrosc.*, 2007, **61**, 1116.
6 C. Meunier, B. Cros and J. Durand, *Journal of Non-Crystalline Solids*, 1994, **169**, 37.
7 A. Dölle, M. A. Suhm and H. Weingärtner, *J. Chem. Phys.*, 1991, **94**, 3361.
8 K. Kneipp, H. Kneipp, R. Manoharan, E. B. Hanlon, I. Itzkan, R. R. Dasari and M. S. Feld, *Appl. Spectrosc.*, 1998, **52**, 1493.
9 T. Park, S. Lee, G. H. Seong, J. Choo, E. K. Lee, Y. S. Kim, W. H. Ji, S. Y. Hwang, D.-H. Gweon and S. Lee, *Lab Chip*, 2005, **5**, 437.
10 M. Wang, N. Jing, I.-H. Chou, G. L. Cote and J. Kameoka, *Lab Chip*, 2007, **7**, 630.
11 H. Xu, E. J. Bjerneld, M. Käll and L. Börjesson, *Phys. Rev. Lett.*, 1999, **83**, 4357.

12 M. Ishikawa, Y. Maruyama, J. Y. Ye and M. Futamata, *J. Lumin.*, 2002, **98**, 81.
13 L. He, M. J. Natan and C. D. Keating, *Anal. Chem.*, 2000, **72**, 5438.
14 P. A. Walker, M. D. Morris, M. A. Burns and B. N. Johnson, *Anal. Chem.*, 1998, **70**, 3766.
15 R. M. Connatser, M. Cochran, R. J. Harrison and M. J. Sepaniak, *Electrophoresis*, 2008, **29**, 1441–1450.
16 L. Chen and J. Choo, *Electrophoresis*, 2008, **29**, 1815–1828.
17 D. L. Jeanmaire and R. P. Van Duyne, *J. Electroanal. Chem.*, 1977, **84**, 1.
18 K. Kneipp, H. Kneipp, I. Itzkan, R. R. Dasari and M. S. Feld, *J. Phys.: Condens. Matter*, 2002, **14**, R597.
19 R. Etchegoin, R. C. Maher, L. F. Cohen, H. Hartigan, R. J. C. Brown, M. J. T. Milton and J. C. Gallop, *Chem. Phys. Lett.*, 2003, **375**, 84.
20 L. A. Dick, A. D. McFarland, C. L. Haynes and R. P. Van Duyne, *J. Phys. Chem. B*, 2002, **106**, 853.
21 G. L. Liu and L. P. Lee, *Appl. Phys. Lett.*, 2005, **87**, 074101.
22 I. M. White, J. Gohring and X. Fan, *Optics Express*, 2007, **15**, 17433.
23 H. Schmidt and A. R. Hawkins, *Microfluid. Nanofluid.*, 2008, **4**, 3.
24 P. Measor, L. Seballos, D. L. Yin, J. Z. Zhang, E. J. Lunt, A. R. Hawkins and H. Schmidt, *Appl. Phys. Lett.*, 2007, **90**, 211107.
25 B. Cordovez, D. Psaltis and D. Erickson, *Appl. Phys. Lett.*, 2007, **90**, 024102.
26 M. Kakuta, F. G. Bessoth and A. Manz, *Chem. Rec.*, 2001, **1**, 395.
27 P. B. Howell, D. R. Mott, S. Fertig, C. R. Kaplan, J. P. Golden, E. S. Oran and F. S. Ligler, *Lab Chip*, 2005, **5**, 524.
28 P. Paik, V. K. Pamula and R. B. Fair, *Lab Chip*, 2003, **3**, 253.
29 N. V. Zaytseva, R. A. Montagna, E. M. Lee and A. J. Baeumner, *Anal. Bioanal. Chem.*, 2004, **380**, 46.
30 A. W. E. Franz, I. Sanchez-Vargas, Z. N. Adelman, C. D. Blair, B. J. Beaty, A. A. James and K. E. Olson, *Proc. Natl. Acad. Sci. USA*, 2006, **103**, 4198.
31 J. F. Hainfeld and R. D. Powell, *J. Histochem. Cytochem.*, 2000, **48**, 471.
32 M. Culha, D. Stokes, L. R. Allain and T. Vo-Dinh, *Anal. Chem.*, 2003, **75**, 6196.
33 K. J. Lee, K. A. Tosser and R. G. Nuzzo, *Adv. Funct. Mater.*, 2005, **15**, 557.
34 A. Nemmar, M. F. Hoylaerts, P. M. Hoet, D. Dinsdale, T. Smith, H. Xu, J. Vermylen and B. Nemery, *Am. J. Respir. Crit. Care Med.*, 2002, **166**, 998.
35 D. Erickson and D. Li, Microscale flow and transport simulation for electrokinetic and lab-on-chip applications, in *Biomems and biomedical nanotechnology*, 2006, vol. 4 (Biomolecular Sensing, Processing and Analysis, R. Bashir and S. Wereley Eds.), Kluwer Academic Publishing.
36 P. Bouriat, P. Saulnier, P. Brochette, A. Graciaa and J. Lachaise, *Journal of Colloid And Interface Science*, 1999, **209**, 445–448.
37 B. J. Kirby and E. F. Hasselbrink Jr., Zeta potential of microfluidic substrates: 2. Data for polymers, *Electrophoresis*, 2004, **25**, 203.
38 K. Faulds, R. E. Littleford, D. Graham, G. Dent and W. E. Smith, *Anal. Chem.*, 2004, **76**, 592–598.
39 S. R. Emory, R. A. Jensen, T. Wenda, M. Han and S. Nie, *Faraday Discussions*, 2006, **132**, 249–259.
40 R. Tantra, R. J. Brown and M. J. Milton, *Journal of Raman Spectroscopy*, 2007, **38**, 1469.
41 D. Lee, S. Lee, G. H. Seong, J. Choo, E. K. Lee, D. G. Gweon and S. Lee, *Applied Spectroscopy*, 2006, **60**, 373–377.
42 W. Plieth, H. Dietz, A. Anders, G. Sandmann, A. Meixner, M. Weber and H. Kneppe, *Surf. Sci.*, 2005, **597**, 119–126.
43 L. L. Gang and P. L. Luke, *Appl. Phys. Lett.*, 2005, **87**, 074101.
44 R. Keir, E. Igata, M. Arundell, W. E. Smith, D. Graham, C. McHugh and J. M. Cooper, *Anal. Chem.*, 2002, **74**, 1503–1508.
45 F. T. Docherty, P. B. Monaghan, R. Keir, D. Graham, W. E. Smith and J. M. Cooper, *Chem. Commun.*, 2004, 118–119.